H2 interaction with divalent cations in isostructural MOFs: a key study for variable temperature infrared spectroscopy

H_2 Interaction with Divalent Cations in Isostructural MOFs: a key study for Variable Temperature Infrared Spectroscopy

Sachin M. Chavan, Olena Zavorotynska, Carlo Lamberti, Silvia Bordiga

Dalton Trans., **2013**, *42*, 12586–12595

doi: 10.1039/c3dt51312b

H_2 Interaction with Divalent Cations in Isostructural MOFs: a key study for Variable Temperature Infrared Spectroscopy

Sachin M. Chavan[ab]*, Olena Zavorotynska[ac], Carlo Lamberti[a], Silvia Bordiga[a*]

Systematic studies of H_2 adsorption by variable temperature infrared (VTIR) spectroscopy have added value in characterization of the hydrogen storage materials. As key study to describe the potentialities of the method, here we report the VTIR spectroscopy results of H_2 adsorption at isostructural MOFs CPO-27-M; (M = Mg, Mn, Co, Ni, Zn,). The strongest perturbation of H_2 vibrational frequency is due to the interaction with open metal site. Although ionic radius is an empirical value, the direct correlation between ionic radii of metal cation and H_2 interaction energy is found in MOFs of same topology. The highest enthalpy of hydrogen adsorption 15 ± 1 kJ mol^{-1} was found for Ni^{2+}.VTIR results of H_2 adsorption in isostructural MOFs CPO-27-M; (M = Mg, Mn, Co, Ni, Zn,) were compared with data obtained in analogue studies performed on a large variety of micropropous materials (MOFs and Zeolites), underlining the relevance of the approach to get reliable energetic values to be compared with computational data and isosteric heats.

1. Introduction

On-board storage of hydrogen for transportation remains one of the challenging barriers on the way to the commercialization of hydrogen-fuelled vehicles. Scientists and engineers have been investigating different pathways to solve this issue.[1-11] Storage of hydrogen by physisorption in microporous materials has shown promising gravimetric and volumetric storage capacity. In general, the H_2 uptake in these materials depends on their surface area at high H_2 pressure and their affinity to H_2 at low hydrogen pressure.[1,4,11,12]

Among the micro porous materials, Metal-organic frameworks (MOFs) are the outstanding hydrogen storage media, due to their extraordinarily high surface areas as well as the tuneable pore sizes and functionality.[2,13-18] MOFs with record surface area have shown very high storage capacity, the highest reported up to date being 176 mg g^{-1} for MOF210 at 77K and 80 bar.[19] However, weak MOF-H_2 interaction imposes impractical cryogenic temperature. Many efforts thus have been applied to the synthesis and/or post-synthetic functionalization of high surface area MOFs with enhanced affinity for molecular hydrogen. [20-23] MOFs with exposed metal sites show higher H_2 affinity than those without.[24,25] This suggests MOFs with very high surface area and exposed metal sites can be the promising materials for hydrogen storage application.[12,26] Authoritative reports clearly underline the need to use quantitative values obtained from H_2 adsorption only on MOFs materials that have been deeply investigated by independent techniques.[12,27] The stability,[28] purity[29] and activation procedure[30] of MOFs are sometimes an issue and accurate measurement of H_2 adsorption is difficult requiring stringent experimental protocols.[12,31-33] Once these points have been settled, an additional important aspect required to probe the materials' affinity for H_2 is to have an insight of hydrogen interaction with the adsorption sites at the molecular level.

Materials for molecular hydrogen storage at laboratory level are mainly characterized by volumetric and gravimetric adsorption isotherms as a function of pressure. These measurements are useful for screening MOFs for the hydrogen storage capacity. Thermodynamics (enthalpy and entropy) of H_2 adsorption is studied by measuring set of adsorption isotherms at different temperatures that gives the isosteric heat of adsorption (Q_{ist}). In this case Q_{ist} is an all-encompassing quantity. Other techniques, such as low temperature programmed desorption (LTPD), low temperature calorimetry of H_2 adsorption, have been used to study the types of adsorption sites and corresponding adsorption heat.[34,35] These techniques are quite demanding and, due to the small values of the measured heats, are subjected to large relative errors. Therefore they are not frequently applied to study the adsorption of hydrogen at MOFs. Inelastic neutron scattering (INS) is widely applied to study H_2 adsorption, but an access to and measurement at the large-scale radiation facilities is time-demanding.[36-50] Finally, Variable Temperature Infrared (VTIR) spectroscopy[51-55] has been widely used to evaluate molecular hydrogen adsorption enthalpy on a large variety of high surface area materials, ranging from porous polymers,[56,57] polycrystalline oxides,[54,55,58] zeolites[55,59-61] and MOFs.[25,55,62-65] VTIR yields accurate site-specific thermodynamic values (standard enthalpy and entropy change), which is an advantage over the calorimetric and volumetric methods. Another very important and unique aspect of VTIR is that it allows for controlling the purity of the adsorbent (as well as hydrogen), since any molecular impurities in the pores of the adsorbent or in the adsorbed gas are readily observable in the infrared spectrum. This assures proper sample activation (e.g. high temperature treatment in vacuum to remove solvent and other impurities from the pores) which is a crucial aspect in the adsorption chemistry of MOFs. Last but not least, being site-specific, among the experimental techniques available to quantify the energy of adsorption, VTIR is particularly suitable for the comparison with results coming from computational techniques, in order to validate the adopted computational approach in terms of functionals, basis-sets, approximation used in the BSSE estimation etc...[63,66] This becomes

particularly evident when a material is characterized by more than one family of sites with similar interaction energy, like MOF-5. In MOF-5 isosteric heat provided an average value between the binding enthalpies of the two sites while VTIR was able to distinguish them (despite the small difference) matching perfectly with quantum mechanical values obtained at very high computational level.[62,67] Conversely, computational data obtained with DFT methods generally underestimate the interaction energy as they do not consider the dispersive part of the interaction. A final aspect that has to be considered is that the experimental values correspond to binding enthalpy, while computed ones are binding energy (zero point energy and thermal contributions needs to be considered before to make a direct comparison between the values).The VTIR method is based on the use of the Van't Hoff equation relating the change in any equilibrium to precisely ΔH^o and ΔS^o and assuming these are independent of temperature. The equilibrium constant of adsorption process is determined from the precise knowledge of intensity of characteristic adsorption band and the corresponding pressure. Brief description of the VTIR experiment and data analysis is given in Section 2.2.2, and for more details see the references.[52,53]Bordiga group was the first to address hydrogen adsorption on MOF-5,[62] HKUST-[25] and CPO-27-Ni[25] followed by VTIR spectroscopy. In particular CPO-27-M framework (also known as MOF-74, M_2(DOBDC), M_2(dhtp)), which shows the highest density of the exposed metal sites, and can be synthesized with different metal ions keeping the same structure, has been investigated by several groups because of its potentialitries in the adsorbtion of different molecules.[23,63,68-73] Zhou et al. studied the role of open metal sites on hydrogen binding on CPO-27-M (M=Mg, Co, Ni and Zn) systems using H_2 adsorption isotherms and theoretical calculations.[23] In later years several reports of VTIR, INS and neutron diffraction of H_2 adsorption at individual CPO-27-M appeared.[45,46,74,75] In particular, INS measurements of H_2 adsorbed on CPO-27M (M= Ni, Co, Mg) samples, by Dietzel et al.[45] showed the presence of a doublet, attributed to different transition from H_2 on the same binding metal site, possibly due to the removal of the degeneration of the $J = 1$ H_2 rotational levels.{Dietzel, 2010 #51} All these reports emphasize the metal sites as the primary and strong H_2 binding sites in the CPO-27-M frameworks. An alternative assignment was given by Chabal et al.[76,77] They claimed that the $H_2 \cdots H_2$ pairing interaction invokes the larger shift in H–H stretching frequency ($\Delta \tilde{\nu}$ (H–H)), whereas H_2 adsorbed at metal sites results in a moderate $\Delta \tilde{\nu}$ (H–H). FitzGerald et al.,[75] however, paid an attention to the fact that the results of Chabal et al. can be due to the poorly activated samples. They performed a very detailed diffuse reflectance infrared Fourier transform (DRIFT) spectroscopic study of H_2 adsorption on completely and partially desolvated CPO-27-M samples. Their finding suggested that the results, reported by Chabal et al.[76,77] are obtained on partially solvated sample.

The live literature debated discussed above justifies the choice of the CPO-27-M series (M= Mg, Mn, Co, Ni, and Zn) as a key study for describing the potentialities of VTIR spectroscopy in transmission mode in gaining quantitative thermodynamic information such as the enthalpy and entropy of H_2 adsorption within MOFs materials. Successively, a comparison on the results of H_2 adsorption on other microporous systems (MOFs with other topologies and zeolites) is reported for discussion.

2. Materials and Methods

2.1. Materials

CPO-27-Mg and CPO-27-Mn were provided by Dr Kenji Sumida (Berkeley Caltech) and Dr Pascal Dietzel (SINTEF) respectively. CPO-27-Co and CPO-27-Ni were prepared in home lab by solvothermal process as reported by Dietzel et al.[68,78] CPO-27-Zn was prepared by following room temperature synthesis procedure reported by Yaghi et al.[79]

2.2. Methods

2.2.1. Powder X-ray diffraction. Samples synthesized in home laboratory were characterized by powder X-ray diffraction. X-ray powder diffraction patterns were collected with a PW3050/60 X'Pert PRO MPD diffractometer from PANalytical working in the Debye–Scherrer geometry, using high-powered ceramic tube PW3373/10 LFF with a Cu anode equipped as a source with a Ni filter to attenuate the Cu K_β line and focused by a PW3152/63 X-ray mirror. Scattered photons were collected by a real time multiple strip X'celerator detector. Powdered samples was placed inside a sealed 1.0 mm boron silicate capillary and mounted on a rotating goniometer head.

2.2.2. Variable Temperature Infrared Spectroscopy: theory. At any given temperature T, the integrated intensity, $A(T)$, of the IR absorption band is proportional to surface coverage, θ, thus giving information on the activity (in the thermodynamic sense) of both the adsorbed species and the empty adsorbing sites. Simultaneously, the equilibrium pressure (p) does the same for the gas phase. Hence, the corresponding adsorption equilibrium constant, K, can be determined, and the variation of K with temperature leads to the corresponding values of adsorption enthalpy and entropy. Assuming Langmuir-type adsorption, we have:[52,53,80]

$$\theta(T) = A(T)/A_M = K(T)\,p\,/\,[1 + K(T)\,p] \qquad (1)$$

where A_M stands for the integrated intensity corresponding to full coverage ($\theta = 1$). Combination of eqn. (1) with the well-known van't Hoff equation (2)

$$K(T) = \exp(-\Delta H^0/RT)\exp(\Delta S^0/R) \qquad (2)$$

leads to eqn. (3):[52,53]

$$\ln[A(T)/(A_M - A(T))p] = (-\Delta H^0/RT) + (\Delta S^0/R)\,. \qquad (3)$$

Defining $Y = \ln[A(T)/(A_M - A(T))p]$, eqn. (3) becomes:

$$Y = (-\Delta H^0/R)\,T^{-1} + (\Delta S^0/R)\,. \qquad (4)$$

Eqn. (4) is the equation of a line in the (Y, T^{-1}) plane, so that different couples of (Y_i, T_i^{-1}) values obtained by VTIR experiments at different temperatures will allow to derive both ΔH^0 and ΔS^0 values through a standard linear fit procedure. Obviously, his approach

assumes a temperature independence of both ΔH^0 and ΔS^0.

2.2.2. Variable Temperature Infrared Spectroscopy: experimental. Thin self-supported wafers of comparable weight and thickness of the MOF samples were prepared and activated (outgassed) in a dynamic vacuum (residual pressure smaller than 10^{-4} mbar) CPO-27-Mn and CPO-27-Co at 423 K for 3 h, CPO-27-Ni at 393K for 2h , CPO-27-Mg at 453K for 18h and CPO-27-Zn at 473 K for 2h to remove solvent completely. After the complete desolvation H_2 (typically 50 mbar) was then dosed at 300 K from a vacuum manifold attached to the IR cryogenic cell. The IR cell had the additional abilities to cool the sample from 300 K down to around 20 K while simultaneously measuring the gas equilibrium pressure. A detailed description of the cryogenic cell (consisting of a modified closed circuit liquid helium Oxford CCC 1204 cryostat) is given elsewhere.[52] FTIR spectra were recorded in transmission mode at 1 cm^{-1} resolution on a Bruker Equinox-55 FTIR spectrometer equipped with an MCT detector. A set of IR spectra were recorded lowering the temperature progressively from 300 to 20 K. Here we report only the spectra obtained at low H_2 coverage in the 200-100 K range, since in all the CPO-27-M the onset adsorption temperature (T_{onset}) is below 200K, and at T < 100K adsorption at the organic linker starts.[25] The hydrogen onset temperature (T_{onset}) is the temperature at which a first IR peak due adsorbed hydrogen appears.

3. CPO-27-M: a key system for VTIR of adsorbed H_2

The IR spectra of the activated CPO-27-M series are reported Fig. 1. The intense absorption peaks in 1700-800 cm^{-1} region are due to the stretching and deformation modes of benzene; symmetric and asymmetric stretching modes of carboxylate (COO^-); and stretching of aryloxy (ArC–O) group of the linker. In a 1700-400 cm^{-1} region IR peaks due to the (C–H) stretching of benzene ring, combinational and overtone modes are observed. The detailed assignment of all vibrational features observed for CPO-27-Ni, is given elsewhere.[69] In the spectra reported here one should pay a particular attention to the absence of intense peaks in 3600-2400 and 1700-1620 cm^{-1} region associated with the modes of water, methanol or DMF that are present in as synthesized samples,[65] and that are virtually absent in the spectra reported in Fig. 1.

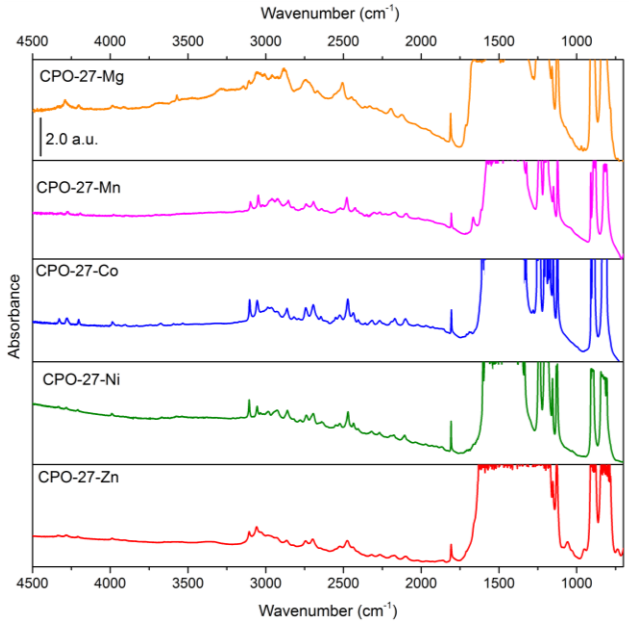

Fig. 1 FTIR spectra of activated CPO-27-M frameworks (before H_2 dosage) are shown. These IR spectra confirm complete desolvation of framework.

Insets in Fig. 2 shows the representative variable temperature IR spectra of H_2 adsorption on CPO-27-M series in the temperature range 200-100 K. H_2 adsorption at low coverage on all CPO-27-M is characterized by the growth of a doublet, red shifted from the gas phase Raman active para-H_2 stretching frequency at $\tilde{\nu}_0$(H-H) = 4161 cm^{-1}. This doublet is assigned to *ortho*-H_2 and *para*-H_2, owing to their expected frequency difference. The appearance of the doublet at a very low H_2 coverage, high T_{onset} with a notable $\Delta\tilde{\nu}$ (H–H) different for each CPO-27-M, indicates H_2 adsorbed at the open metal sites. Since all the MOFs in the CPO-27-M series contain same organic linker, interaction with it causes similar shift in $\tilde{\nu}$ (H-H), from –20 to –40 cm^{-1}, and is observed bellow 100 K only.

As described in Section 2.2.2, the integrated intensity $A(T)$ of IR peak due to H_2 adsorbed at M^{2+} sites, together with simultaneously recorded values of temperature and pressure inside the closed IR cell, is used to determine the ΔH^0 and ΔS^0 of H_2 adsorption, see eqn (3), (4).

Fig. 2 shows the Van't Hoff plot obtained for the $A(T)$ obtained from the IR spectra shown in the insets. The obtained values of ΔH^0, ΔS^0, T_{onset}, and of the $\Delta\tilde{\nu}$ (H-H) shift are reported in Table 1. The estimated error limits are ± 1 kJ mol^{-1} for enthalpy and ± 10 $Jmol^{-1}K^{-1}$ for the entropy.[80] Within the experimental error ΔH^0 values obtained by VTIR are similar to the values found by H_2 adsorption isotherms and by neutron diffraction. As expected, greater ΔH^0 values are associated with larger ΔS^0, vide infra the general discussion in Section 4.

Table 1. Summary of the results obtained in this work by VTIR, $\Delta\tilde{\nu}$ (H-H) in cm^{-1} is calculated with respect to the Raman stretching frequency $\tilde{\nu}$ (H-H) of *para* –H_2 in the gas phase which is 4161 cm^{-1}. In the last two columns, ΔH^o values obtained in this work are compared with VTIR, and isosteric heat of adsorption (Q_{ist}) from the literature. Ionic radii (R_M) for $M^{2+}{}_{5C}$ are taken from the compilation of Shannon.{Shannon, 1976 #52}

CPO-27-M	$\tilde{\nu}$ (H-H) (cm^{-1})	$-\Delta\tilde{\nu}$ (H-H) (cm^{-1})	T_{onset} (K)	$-\Delta H^0$ (kJmol^{-1})	$-\Delta S^0$ (J mol^{-1} K^{-1})	R_M (Å)	$-\Delta H$ literature	
							VTIR (kJ mol^{-1})	Q_{ist} (kJ mol^{-1})
Mg^{2+}	4086 4092	75 69	139	12 ± 1	137 ± 10	0.66	9.4±1 [a]	10.1 [b]
Mn^{2+}	4081 4088	80 73	129	11 ± 1	122 ± 10	0.75	-	8.8 [b]
Co^{2+}	4041 4046	120 115	158	13 ± 1	146 ± 10	0.67	11.2±1 [c]	10.7 [b]
Ni^{2+}	4030 4036	131 125	180	15 ± 1	170 ± 10	0.63	13.0±1 [d]	12.9 [b]
Zn^{2+}	4089 4095	72 66	120	10 ± 1	137 ± 10	0.68	-	8.5 [b]

[a] Ref.[46]; [b] Ref. [23]; [c] Ref. [74]; [d] Ref. [25]

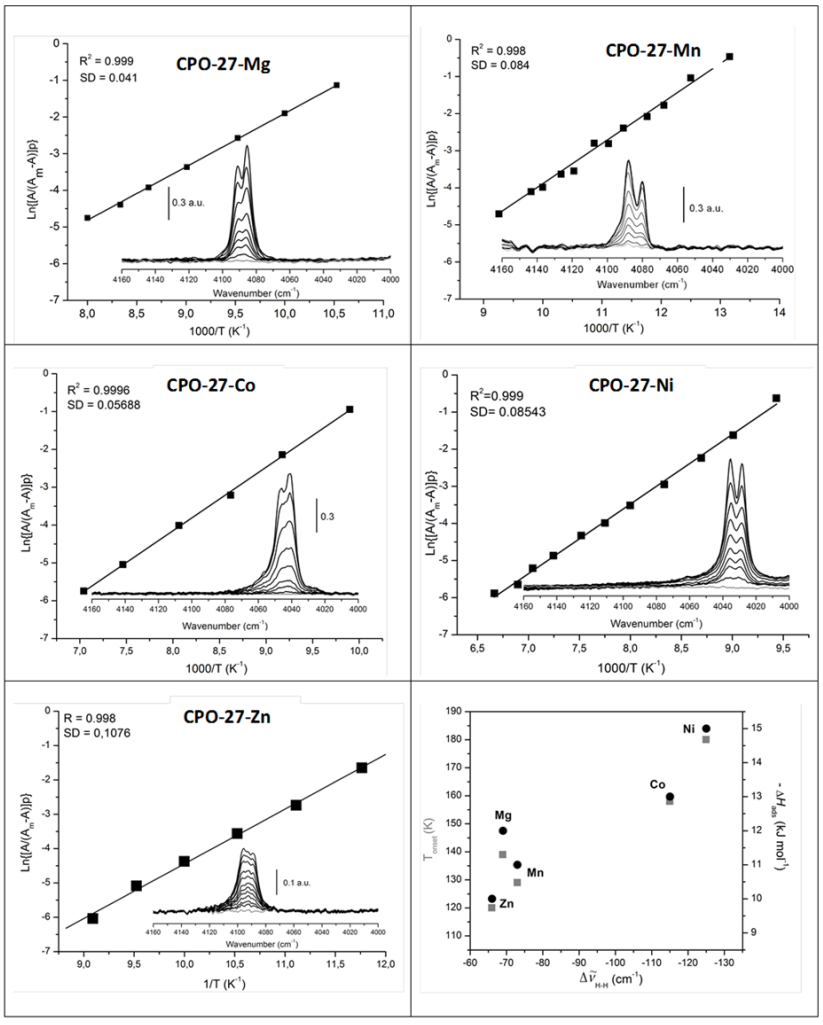

Fig. 2. Insets report the VTIR spectra of H_2 adsorbed on properly desolvated CPO-27-M series in the temperature range 200-100 K. The Main parts report the *Van't Hoff* plots obtained from the VTIR data reported in the insets as described in Section 2.2.2.. Bottom right plots show the relationship between T_{onset}, $\Delta\tilde{\nu}$ (H-H) and ΔH^o. The frequency of the Raman active mode of *para*-H_2, $\tilde{\nu}_0$(H-H) = 4161 cm^{-1}, is used as a reference to calculate $\Delta\tilde{\nu}$ (H-H). Also reported in the goodness factor of the linear fit (R) and the corresponding standard deviation (SD).

A linear relation is observed for both T_{onset} and $-\Delta H^0$ vs. $\Delta \tilde{\nu}$ (H-H) (see last panel in Fig. 2). The liner correlation between T_{onset} and ΔH^0 is reported in Fig. 3. The linear fit of the experimental data results in:

$$- \Delta H^0 = 0.080(5)\ (\text{J mol}^{-1}\ \text{K}^{-1})\ T_{onset} + 0.6(7)\ \text{kJ mol}^{-1} \qquad (5)$$

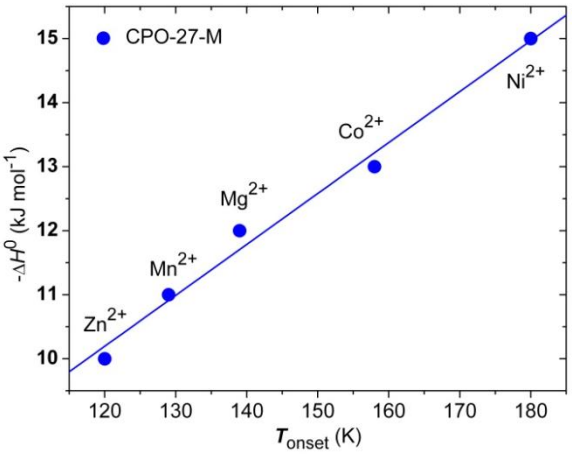

Fig. 3. Linear relation between $-\Delta H^0$ values obtained from the VTIR experiments reported in Fig.2 and T_{onset}. Experimental data: scattered circles; best linear fit: blue line (R = 0.994 σ = 0.245 kJ/mol

The value of 0.6 ± 0.7 kJ mol^{-1}, obtained in the fit (5), is compatible with the expected limit of $-\Delta H^0$ to zero when T_{onset} is approaching 0 K. The behaviours reported in the last panel of Fig. 2 and in Fig. 3 are characteristic of isostructural frameworks. Such relationship deviates from the linearity when different framework topologies are considered.[60,81] Based on the enthalpy of adsorption and T_{onset}, the trends in H_2 binding for the CPO-27-M series follow the order: Ni > Co > Mg > Mn > Zn.

A correlation also exists for both $-\Delta \tilde{\nu}$ (H-H) and $-\Delta H^0$ versus $(R_M)^{-2}$, being R_M the ionic radius of the metal site, see Fig. 4. These correlations are however less well defined than in the case of $-\Delta \tilde{\nu}$ (H-H) and $-\Delta H^0$ versus T_{onset}. The data reported in Fig. 4 are in qualitative agreement with the findings of Zhou et al.[23] that in isostructural material the affinity of the material for H_2 can be predicted on the basis of the R_M of exposed metal sites. The data reported in Fig. 4 confirm that the major interaction between the open metal centre and the H_2 molecule is of Coulomb nature, however this hold in first approximation only, and for isostructural frameworks only i.e. in cases when the local environment around the metal site remains the same changing metal.

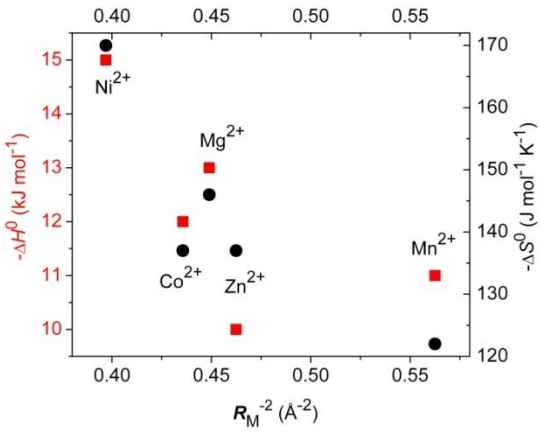

Fig. 4. Correlation between $-\Delta H^0$ (red squares, left ordinate axis) and $-\Delta S^0$ (black circles, right ordinate axis) values obtained from the VTIR experiments reported in Fig.2 and the inverse of the squared cationic radius of the metal canter.

Comparison of CPO-27-Ni with a MOF STA-12-Ni,[82] which is structurally similar to CPO-27-Ni, evidences the importance of coordination environment in hydrogen adsorption at the metal site. Both CPO-27-Ni and STA-12 in activated form contain edge sharing five coordinated metal centres with only difference in the coordination environment, which is "NiO_5" in CPO-27-Ni and "NiO_4N" in

STA-12-Ni. The H_2 adsorbed on Ni site in STA-12 gives IR signals at 4107 and 4119 cm^{-1}.[82] This frequency shift is less than that observed for CPO-27-Ni, indicating that Ni^{2+} in STA-12 polarizes H_2 to a lower extent than Ni^{2+} in CPO-27-Ni. The enthalpy of H_2 adsorption on STA-12-Ni is correspondingly 7.5 kJ $mole^{-1}$.

4. Comparison with VTIR data of H_2 adsorbed on other microporous frameworks

Table 2 summarizes literature results obtained using VTIR in the study of H_2 adsorption on different microporous materials. Fig. 5 shows the relationship between the $-\Delta H^0$ and $-\Delta S^0$ data reported in the data summarized in both Tables 1 and 2. The overall data do not show a commune trend, nevertheless, if we consider separately some sub-sets of data, particular trends can be identified. (i) $-\Delta H^0$ and $-\Delta S^0$ exhibit both a strong dependence on the particular microporous material used in the adsorption, and (iii) within the same class of adsorbing materials there is a positive correlation between enthalpy and entropy:

$$-\Delta H^0 \; \alpha \; -\Delta S^0 \qquad (6)$$

Table 2. Summary of the literature results obtained using VTIR in the study of H_2 adsorption on different microporous materials. $\Delta\tilde{\nu}$ (H-H) in cm^{-1} is calculated with respect to the Raman stretching frequency $\tilde{\nu}$ (H-H) of *para* –H_2 in the gas phase which is 4161 cm^{-1}. Ionic radii (R_M) are taken from the compilation of Shannon{Shannon, 1976 #52} considering both the cation charge and its coordination, given as roman number in parenthesis. NR = not reported.

Material	Cation charge (Coord.)	$\tilde{\nu}$ (H-H) (cm^{-1})	$-\Delta\tilde{\nu}$ (H-H) (cm^{-1})	$-\Delta H^0$ (kJ/mol)	$-\Delta S^o$ (J mol^{-1} K^{-1})	R_M (Å)	Ref.
$Cu_2(BTC)_3$	Cu^{2+}(IV)	4090, 4097	71, 64	10 ± 1	169 ± 10	0.57	[25]
MIL-101	Cr^{3+}(V)	4066	95	9.5 ± 1	112 ± 10	0.61	[80]
MIL-100	Cr^{3+}(V)	4050	111	6.9 ± 1	80 ± 10	0.61	[80]
MIL-100	Sc^{3+}(V)	4082	79	11.2 ± 1	120 ± 10	0.74	[61]
Fe-BTT	Fe^{2+}(V)	3980	181	12.9 ± 1	68 ± 10	0.61	[93]
Cu-BTT	Cu^{2+}(V)	4058, 4065	103, 96	10.4 ± 1	66 ± 10	0.57	[93]
Mn-BTT	Mn^{2+}(V)	4038	123	11.9 ± 1	68 ± 10	0.75	[93]
Li-ZSM-5	Li^{+}(IV)	4092	69	6.5 ± 1	90 ± 10	0.59	[94]
Na-ZSM-5	Na^{+}(IV)	4101	60	10.3 ± 1	121 ± 10	0.99	[94]
K-ZSM-5	K^{+}(IV)	4112	49	9.1 ± 1	124 ± 10	1.37	[94]
Cu-ZSM-5	Cu^{+}	3130, 3079	1031, 1082	60-80	NR	0.60	[59]
Li-FER	Li^{+}(IV)	4090	71	4.1 ± 1	57 ± 10	0.59	[95]
Na-FER	Na^{+}(IV)	4100	61	6.0 ± 1	78 ± 10	0.99	[95]
K-FER	K^{+}(IV)	4111	50	3.5 ± 1	57 ± 10	1.37	[95]
Ca-FER	Ca^{2+}	4083	78	12 ± 1	121 ± 10	1.00	[95]
H-SSZ-13	H^{+}	4090	71	9.7± 1	NR	-	[96]
Na-A	Na^{+}(IV)	4072	89	12.9 ± 1	NR	0.99	[60]
Ca-A	Ca^{2+}	4085	76	13.0± 1	NR	1.00	[60]
Mg-Na-Y	Mg^{2+}	4056	105	17.5 ± 1	136± 10	0.57	[97]
Ca-Na-Y	Ca^{2+}	4078	83	15 ± 1	127± 10	1.00	[98]
Na-X	Na^{+}(IV)	4066	95	11 ± 1	103± 10	0.99	[98]
Mg-X	Mg^{2+}	4065	96	13 ± 1	114 ± 10	0.57	[99]
Ca-X	Ca^{2+}	4082	79	12.5 ± 1	118 ± 10	1.00	[98]

Besides H_2 adsorption in zeolites,[80,83] such trend, already referred to as entropy–enthalpy compensation, was observed in the literature for a range of chemical processes involving weak interaction forces such as the formation of weakly associated molecular complexes,[84,85] weak hydrogen bonding[86,87] and Langmuir-type adsorption from solution.[86]

The $-\Delta H^0 \; \alpha \; -\Delta S^0$ correlation is related to the fact that the stronger the interaction between hydrogen molecules and the adsorbing centre is, the greater will be the corresponding decrease of H_2 motion freedom, which results in an increasing order of the system. Hence, referring to absolute values, a greater $-\Delta H^0$ will result in a correspondingly greater $-\Delta S^0$.[80,83]

In two recent contributions, Otero Arean and Garrone,[80,83] showed that within zeolites and Cr-MIL MOFs the enthalpy–entropy correlation ($-\Delta H^0 \; \alpha \; -\Delta S^0$) does not follow a straight line, but a concave curve. This trend was explained as follows: the adsorbed H_2 molecules cannot lose more than all of their degrees of freedom of motion, $-\Delta S^0$ has consequently an inherent limit, whereas (in principle) $-\Delta H^0$ has not. The $-\Delta S^0$ limit is not reached in the adsorption process, because some rotational and vibrational freedom (against the adsorption site) remains in the adsorbed state.

The summary of the data obtained on zeolites (red stars in Fig. 5), representing a larger dataset with respect to that considered in the works of Otero Arean and Garrone,[80,83] confirm their model as a steep increase in $-\Delta H^0$ is observed when $-\Delta S^0$ approaches values as high as 110-130 J mol^{-1} K^{-1}.

The behaviour observed for Cr-MIL, Sc-MIL and CPO-27-M MOFs (black and blue circles in Fig. 3) exhibits an almost linear trend in

the large interval of $-\Delta S^0$, spanning from 80 to 170 J mol^{-1} K^{-1}. The latter value, observed for CPO-27-Ni, approaches the limit of $-\Delta S^0$ = 180 J mol^{-1} K^{-1}. Foreseen for 1 mol of hydrogen at 1 Torr and 100 K who will completely lose its degrees of freedom.[80]

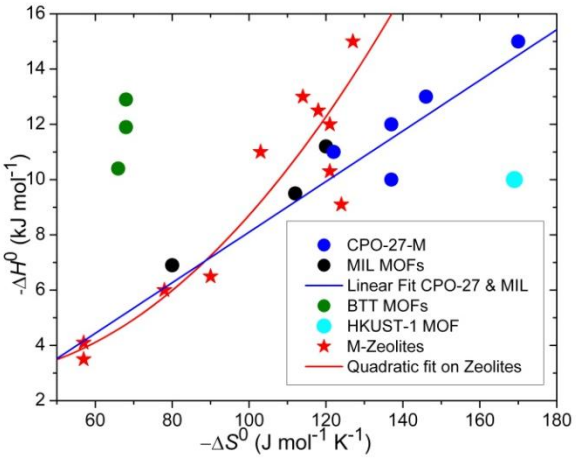

Fig. 5. Correlation between $-\Delta H^0$ and $-\Delta S^0$. The data, reported from Table 1 and 2, refer to CPO-27-M MOFs (blue circles), MIL MOFs (black circles), BTT MOFs (green circles), HKUST-1 MOF (cyan circle) and M-zeolites (red stars). The blue line represents the best linear fit of the MIL and CPO-27 data. The red curve is the best quadratic fit on the zeolite data.

The values for BTT MOFs lies in a completely different region of the ($-\Delta S^0$,$-\Delta H^0$) plane: low entropy, high enthalpy region. This peculiarity is related to the different ligands present in BTT MOFs (1,3,5-benzenetritetrazolate), where N atoms are in the first coordination shell of the metal ions and where also Cl^- anions are present. This confirms that the link through the N atoms change substantially the polarizing power of the cations. On the opposite side of the plane (high entropy, low enthalpy region) lies the HKUST-1 material.

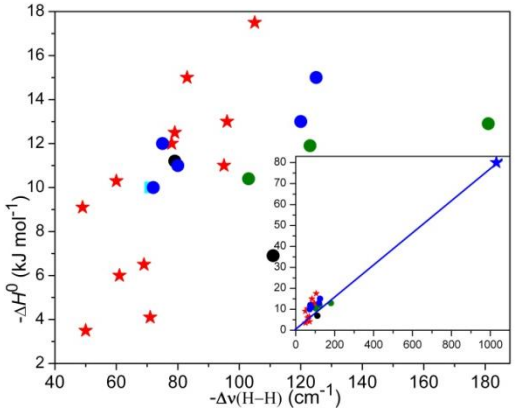

Fig. 6. Correlation between $-\Delta H^0$ and $^{-\Delta}\tilde{\nu}$ (H-H). The data, reported from Table 1 and 2, refer to CPO-27-M MOFs (blue circles), MIL MOFs (black circles), BTT MOFs (green circles), HKUST-1 MOF (cyan circle), Cu^+-ZSM-5 (blue star) all remaining M-zeolites (red stars). The inset reports an enlarged region allowing to observe also the datum referred to Cu^+-ZSM-5. The blue line is the line joining the origin with the point referred to Cu^+-ZSM-5 zeolite.

Fig. 6 reports the correlation between $-\Delta H^0$ and $^{-\Delta}\tilde{\nu}$ (H-H) on the whole set of data reported in Tables 1 and 2. Although characterized by a large spread, the data basically show that a large $^{-\Delta}\tilde{\nu}$ (H-H) corresponds to a large $-\Delta H^0$. This general trend holds also for Cu^+-ZSM-5 case, that exhibits $-\Delta H^0$ and $^{-\Delta}\tilde{\nu}$ (H-H) values as high as 80 kJ mol^{-1} and 1082 cm^{-1}, respectively. In this regard, the theoretical analysis of the components of the adsorption energy, revealed that charge transfer from the Cu($3d_\pi$) orbital through the antibonding $H_2(\sigma_u)$ and orbital polarization play a significant role in the H_2 adsorption energy, and is the cause of the so large bathochromic H_2 frequency shift.[88]

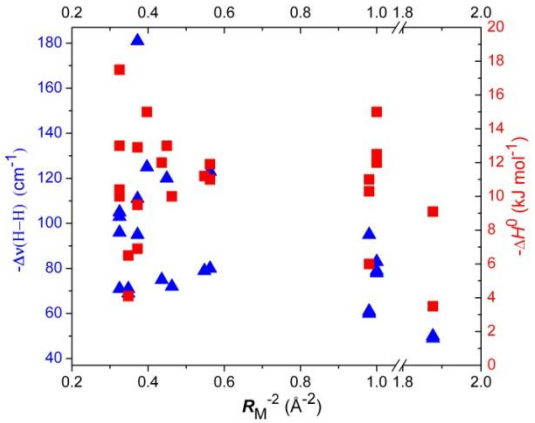

Fig. 7. Values of $-\Delta H^0$ (red squares, right ordinate axis) and of $-\Delta\tilde{\nu}$ (H-H) (blue triangles, left ordinate axis) reported as a function of the inverse of the square of the cation ionic radius (R_M).

We conclude the analysis of the data summarized in Tables 1 and 2 by trying to reproduce for H_2 the simple linear relation between frequency shift and $(R_M)^{-2}$ that was observed for CO adsorbed on non-d metal centres.[55,89-91] Fig. 7 reports the values of $-\Delta H^0$ (red squares, right ordinate axis) and of $-\Delta\tilde{\nu}$ (H-H) (blue triangles, left ordinate axis) as a function of $(R_M)^{-2}$. From the data reported in Fig. 7, the lack of any correlation is evident. H_2 clearly behaves differently than CO, because while CO interacts with the cation mainly, H_2 interacts with both the cation and its anionic counterparts.[92] The weak correlation between of $-\Delta H^0$ and $(R_M)^{-2}$ observed in Fig. 4 when the data referred to CPO-27-M samples only is completely lost when the other data are included in the plot. The difference in the anionic counterparts and in the cationic local environment makes

5. Conclusion

In summary, in the CPO-27-M MOFs series, CPO-27-Ni has shown the strongest perturbation of H_2 vibrational frequency with the adsorption enthalpy 15 ± 1 kJ mol^{-1}. This is the highest reported value for H_2 adsorption in metal-organic framework. Our results confirm the role of metal site as the primary binding site for H_2 adsorption at CPO-27-M framework. Metal sites are the one responsible for strong perturbation of H_2 vibrational frequency and not the $H_2\cdots H_2$ pairing interaction. A linear relationship observed between T_{onset}, $\Delta\tilde{\nu}$ (H-H) and ΔH^0 radii can be used in the design of isostuctural materials with high hydrogen affinity. The thermodynamic data obtained from this VTIR study on CPO-27-M MOFs was then compared with the VTIR data available in literature on MOFs and zeolites. The obtained overall picture is extremely complex and can be rationalized only dividing the samples into subsets characterized by the difference in the local environment, particularly the first shell anions, surrounding the metal centre that act as adsorbing site for H_2.

ACKNOWLEDGMENT

We thank Pascal C. Dietzel and Kenji Sumida for providing MOF-74-Mg and CPO-27-Mn sample respectively. We acknowledge the financial support by "Progetti di Ricerca di Ateneo-Compagnia di San Paolo-2011- Linea 1A", ORTO11RRT5 project.

Notes and references

[a]*Chemistry Department, NIS, centre of Exchellence and INSTM università di Torino, via Pietro Giuria 7 and via Quarello 11, 10100, Torino, Italy* silvia.bordiga@unito.it

[b]*Department of Chemistry, University of Oslo , P.O. Box 1033 Blindern, N-0315, Oslo, Norway, Email:* Sachin.chavan@kjemi.uio.no

[c]*Institute for Energy Technology, Instituttveien 18, P.O. Box 40, N-2027, Kjeller, Norway*

† Electronic Supplementary Information (ESI) available: XRPD of in home laboratory synthesized CPO-27-M are given in supporting information.

TOC text and figure

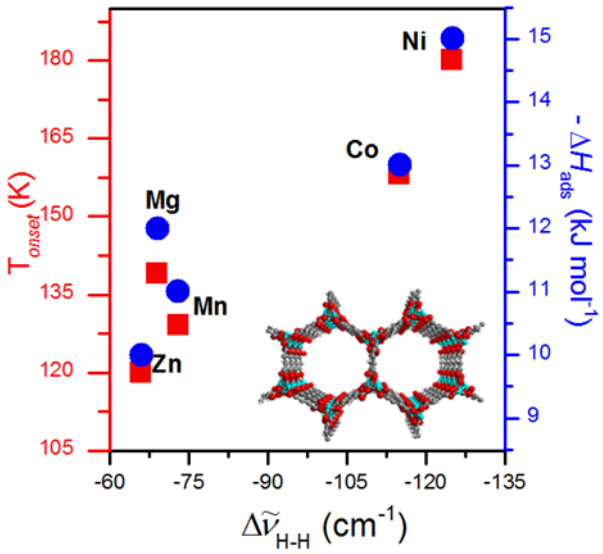

Systematic studies of H_2 adsorption at isostructural MOFs CPO-27-M; (M = Mg, Mn, Co, Ni, Zn,) is followed by variable temperature infrared (VTIR) spectroscopy. A linear relationship observed between T_{onset}, $\Delta\tilde{\nu}$ (H-H), ΔH^o and ionic radii can be used in the design of isostuctural materials with high hydrogen affinity.

References

1 B. Panella and M. Hirscher, *Adv. Mater.*, 2005, **17**, 538.

2 A. G. Wong-Foy, A. J. Matzger and O. M. Yaghi, *J. Am. Chem. Soc.*, 2006, **128**, 3494.

3 M. Hirscher, *Handbook of Hydrogen Storage*; 1 ed.; Wiley-VCH, : Weinheim, **2010**.

4 Y. H. Hu and L. Zhang, *Adv. Mater.*, 2010, **22**, E117.

5 P. Jena, *J. Phys. Chem. Lett.*, 2011, **2**, 206.

6 S. W. Jorgensen, *Curr. Opin. Solid St. M.*, 2011, **15**, 39.

7 S. Ma and H.-C. Zhou, *Chem. Commun.*, 2010, **46**, 44.

8 K. Mazloomi and C. Gomes, *Renew. Sust. Energ. Rev.*, 2012, **16**, 3024.

9 S. McWhorter, C. Read, G. Ordaz and N. Stetson, *Curr. Opin. Solid St. M.*, 2011, **15**, 29.

10 J. Sculley, D. Yuan and H.-C. Zhou, *Energ. Environ. Sci.*, 2011, **4**, 2721.

11 M. P. Suh, H. J. Park, T. K. Prasad and D.-W. Lim, *Chem. Rev.*, 2012, **112**, 782.

12 K. M. Thomas, *Dalton Trans.*, 2009, 1487.

13 S. Chavan, *Characterization of Metal-organic Frameworks for Gas Storage and Catalysis applications*, PhD thesis in Materials Science, University of Turin (I), **2010**

14 S. L. James, *Chem. Soc. Rev.*, 2003, **32**, 276.

15 J. L. C. Rowsell, A. R. Millward, K. S. Park and O. M. Yaghi, *J. Am. Chem. Soc.*, 2004, **126**, 5666.

16 J. L. C. Rowsell and O. M. Yaghi, *Angew. Chem.-Int. Edit.*, 2005, **44**, 4670.

17 B. Xiao, P. S. Wheatley, X. B. Zhao, A. J. Fletcher, S. Fox, A. G. Rossi, I. L. Megson, S. Bordiga, L. Regli, K. M. Thomas and R. E. Morris, *J. Am. Chem. Soc.*, 2007, **129**, 1203.

18 M. Dincă and J. R. Long, *Angew. Chem.-Int. Edit.*, 2008, **47**, 6766.

19 H. Furukawa, N. Ko, Y. B. Go, N. Aratani, S. B. Choi, E. Choi, A. O. Yazaydin, R. Q. Snurr, M. O'Keeffe, J. Kim and O. M. Yaghi, *Science*, 2010, **329**, 424.

20 H. J. Park and M. P. Suh, *Chem. Commun.*, 2012, **48**, 3400.

21 Z. Wang, K. K. Tanabe and S. M. Cohen, *Chem. Euro. J.*, 2010, **16**, 212.

22 J. Yang, A. Grzech, F. M. Mulder and T. J. Dingemans, *Chem. Commun.*, 2011, **47**, 5244.

23 W. Zhou, H. Wu and T. Yildirim, *J. Am. Chem. Soc.*, 2008, **130**, 15268.

24 M. Dinca, A. Dailly, Y. Liu, C. M. Brown, D. A. Neumann and J. R. Long, *J. Am. Chem. Soc.*, 2006, **128**, 16876.
25 J. G. Vitillo, L. Regli, S. Chavan, G. Ricchiardi, G. Spoto, P. D. C. Dietzel, S. Bordiga and A. Zecchina, *J. Am. Chem. Soc.*, 2008, **130**, 8386.
26 L. J. Murray, M. Dinca and J. R. Long, *Chem. Soc. Rev.*, 2009, **38**, 1294.
27 G. Ferey, *Chem. Soc. Rev.*, 2008, **37**, 191.
28 S. S. Kaye, A. Dailly, O. M. Yaghi and J. R. Long, *J. Am. Chem. Soc.*, 2007, **129**, 14176.
29 J. Hafizovic, M. Bjorgen, U. Olsbye, P. D. C. Dietzel, S. Bordiga, C. Prestipino, C. Lamberti and K. P. Lillerud, *J. Am. Chem. Soc.*, 2007, **129**, 3612.
30 J. C. Liu, J. T. Culp, S. Natesakhawat, B. C. Bockrath, B. Zande, S. G. Sankar, G. Garberoglio and J. K. Johnson, *J. Phys. Chem. C*, 2007, **111**, 9305.
31 D. P. Broom, *Int. J. Hydrog. Energy*, 2007, **32**, 4871.
32 D. P. Broom and P. Moretto, *J. Alloy. Compd.*, 2007, **446**, 687.
33 K. M. Thomas, *Catal. Today*, 2007, **120**, 389.
34 M. J. Blandamer, P. M. Cullis and P. T. Gleeson, *Chem. Soc. Rev.*, 2003, **32**, 264.
35 P. M. Forster, J. Eckert, B. D. Heiken, J. B. Parise, J. W. Yoon, S. H. Jhung, J. S. Chang and A. K. Cheetham, *J. Am. Chem. Soc.*, 2006, **128**, 16846.
36 N. L. Rosi, J. Eckert, M. Eddaoudi, D. T. Vodak, J. Kim, M. O'Keeffe and O. M. Yaghi, *Science*, 2003, **300**, 1127.
37 J. L. C. Rowsell, J. Eckert and O. M. Yaghi, *J. Am. Chem. Soc.*, 2005, **127**, 14904.
38 Y. L. Liu, J. F. Eubank, A. J. Cairns, J. Eckert, V. C. Kravtsov, R. Luebke and M. Eddaoudi, *Angew. Chem.-Int. Edit.*, 2007, **46**, 3278.
39 F. M. Mulder, B. Assfour, J. Huot, T. J. Dingemans, M. Wagemaker and A. J. Ramirez-Cuesta, *J. Phys. Chem. C*, 2010, **114**, 10648.
40 F. M. Mulder, T. J. Dingemans, H. G. Schimmel, A. J. Ramirez-Cuesta and G. J. Kearley, *Chem. Phys.*, 2008, **351**, 72.
41 C. M. Brown, Y. Liu, T. Yildirim, V. K. Peterson and C. J. Kepert, *Nanotechnology*, 2009, **20**, Art. n. 204025.
42 L. Z. Kong, G. Roman-Perez, J. M. Soler and D. C. Langreth, *Phys. Rev. Lett.*, 2009, **103**, Art. n. 096103.
43 S. A. FitzGerald, J. Hopkins, B. Burkholder, M. Friedman and J. L. C. Rowsell, *Phys. Rev. B*, 2010, **81**, Art. n. 104305.
44 N. R. Stuckert, L. F. Wang and R. T. Yang, *Langmuir*, 2010, **26**, 11963.
45 P. D. C. Dietzel, P. A. Georgiev, J. Eckert, R. Blom, T. Straessle and T. Unruh, *Chem. Commun.*, 2010, **46**, 4962.
46 K. Sumida, C. M. Brown, Z. R. Herm, S. Chavan, S. Bordiga and J. R. Long, *Chem. Commun.*, 2011, **47**, 1157.
47 S. H. Yang, S. K. Callear, A. J. Ramirez-Cuesta, W. I. F. David, J. L. Sun, A. J. Blake, N. R. Champness and M. Schroder, *Faraday Discuss.*, 2011, **151**, 19.
48 L. F. Wang, N. R. Stuckert, H. Chen and R. T. Yang, *J. Phys. Chem. C*, 2011, **115**, 4793.
49 D. J. Tranchemontagne, K. S. Park, H. Furukawa, J. Eckert, C. B. Knobler and O. M. Yaghi, *J. Phys. Chem. C*, 2012, **116**, 13143.
50 I. Matanovic, J. L. Belof, B. Space, K. Sillar, J. Sauer, J. Eckert and Z. Bacic, *J. Chem. Phys.*, 2012, **137**, Art. n. 014701.
51 E. A. Paukshtis and E. N. Yurchenko, *Russ. Chem. Rev.*, 1983, **52**, 242.
52 G. Spoto, E. N. Gribov, G. Ricchiardi, A. Damin, D. Scarano, S. Bordiga, C. Lamberti and A. Zecchina, *Prog. Surf. Sci.* , 2004, **76**, 71.
53 E. Garrone and C. Otero Arean, *Chem. Soc. Rev.*, 2005, **34**, 846.
54 C. Lamberti, E. Groppo, G. Spoto, S. Bordiga and A. Zecchina, *Adv. Catal.*, 2007, **51**, 1.
55 C. Lamberti, E. Groppo, A. Zecchina and S. Bordiga, *Chem. Soc. Rev.*, 2010, **39**, 4951.
56 G. Spoto, J. G. Vitillo, D. Cocina, A. Damin, F. Bonino and A. Zecchina, *Phys. Chem. Chem. Phys.*, 2007, **9**, 4992.
57 J. Estephane, E. Groppo, J. G. Vitillo, A. Damin, C. Lamberti, S. Bordiga and A. Zecchina, *Phys. Chem. Chem. Phys.*, 2009, **11**, 2218.
58 E. N. Gribov, S. Bertarione, D. Scarano, C. Lamberti, G. Spoto and A. Zecchina, *J. Phys. Chem. B*, 2004, **108**, 16174.
59 G. Spoto, E. Gribov, S. Bordiga, C. Lamberti, G. Ricchiardi, D. Scarano and A. Zecchina, *Chem. Commun.*, 2004, 2768.
60 O. Zavorotynska, J. G. Vitillo, G. Spoto and A. Zecchina, *Int. J. Hydrogen. Energ.*, 2011, **36**, 7944.
61 C. Otero Arean, C. Palomino Cabello and G. Turnes Palomino, *Chem. Phys. Lett.*, 2012, **521**, 104.
62 S. Bordiga, J. G. Vitillo, G. Ricchiardi, L. Regli, D. Cocina, A. Zecchina, B. Arstad, M. Bjorgen, J. Hafizovic and K. P. Lillerud, *J. Phys. Chem. B*, 2005, **109**, 18237.
63 L. Valenzano, J. G. Vitillo, S. Chavan, B. Civalleri, F. Bonino, S. Bordiga and C. Lamberti, *Catal. Today*, 2012, **182**, 67.
64 S. Chavan, J. G. Vitillo, D. Gianolio, O. Zavorotynska, B. Civalleri, S. Jakobsen, M. H. Nilsen, L. Valenzano, C. Lamberti, K. P. Lillerud and S. Bordiga, *Phys. Chem. Chem. Phys.*, 2012, **14**, 1614.
65 F. Bonino, C. Lamberti, S. Chavan, J. G. Vitillo and S. Bordiga, *Characterization of MOFs by combined vibrational, and electronic spectroscopies*, in: Metal-Organic Frameworks in heterogeneous catalysis; F. X. Llabrés i Xamena and J. Gascón, Ed.; RSC: Cambridge, **2013**.
66 L. Valenzano, B. Civalleri, S. Chavan, G. T. Palomino, C. O. Arean and S. Bordiga, *J. Phys. Chem. C*, 2010, **114**, 11185.
67 K. Sillar, A. Hofmann and J. Sauer, *J. Am. Chem Soc.*, 2009, **131**, 4143.
68 P. D. C. Dietzel, B. Panella, M. Hirscher, R. Blom and H. Fjellvag, *Chem. Commun.*, 2006, 959.
69 F. Bonino, S. Chavan, J. G. Vitillo, E. Groppo, G. Agostini, C. Lamberti, P. D. C. Dietzel, C. Prestipino and S. Bordiga, *Chem. Mater.*, 2008, **20**, 4957.
70 S. R. Caskey, A. G. Wong-Foy and r. A. J. Matzge, *J. Am. Chem. Soc.* , 2008, **130**, 10870.
71 S. Chavan, F. Bonino, J. G. Vitillo, E. Groppo, C. Lamberti, P. D. C. Dietzel, A. Zecchina and S. Bordiga, *Phys. Chem. Chem. Phys.*, 2009, **11**, 9811.
72 S. Chavan, J. G. Vitillo, E. Groppo, F. Bonino, C. Lamberti, P. D. C. Dietzel and S. Bordiga, *J. Phys. Chem. C*, 2009, **113**, 3292.
73 H. Wu, W. Zhou and T. Yildirim, *J. Am. Chem. Soc*, 2009, **131**, 4995.
74 C. O. Arean, S. Chavan, C. P. Cabello, E. Garrone and G. T. Palomino, *ChemPhysChem*, 2010, **11**, 3237.

75 S. A. FitzGerald, B. Burkholder, M. Friedman, J. B. Hopkins, C. J. Pierce, J. M. Schloss, B. Thompson and J. L. C. Rowsell, *J. Am. Chem. Soc.*, 2011, **133**, 20310.
76 N. Nijem, J.-F. Veyan, L. Kong, K. Li, S. Pramanik, Y. Zhao, J. Li, D. Langreth and Y. J. Chabal, *J. Am. Chem. Soc.*, 2010, **132**, 1654.
77 N. Nijem, J.-F. Veyan, L. Kong, H. Wu, Y. Zhao, J. Li, D. C. Langreth and Y. J. Chabal, *J. Am. Chem. Soc.*, 2010, **132**, 14834.
78 P. D. C. Dietzel, R. E. Johnsen, R. Blom and H. Fjellvåg, *Chem. Eur. J.*, 2008, **14**, 2389.
79 D. J. Tranchemontagne, J. R. Hunt and O. M. Yaghi, *Tetrahedron*, 2008, **64**, 8553.
80 G. Turnes Palomino, C. Palomino Cabello and C. Otero Arean, *Eur. J. Inorg. Chem.*, 2011, 1703.
81 L. Regli, A. Zecchina, J. G. Vitillo, D. Cocina, G. Spoto, C. Lamberti, K. P. Lillerud, U. Olsbye and S. Bordiga, *Phys. Chem. Chem. Phys.*, 2005, **7**, 3197.
82 S. R. Miller, G. M. Pearce, P. A. Wright, F. Bonino, S. Chavan, S. Bordiga, I. Margiolaki, N. Guillou, G. Ferey, S. Bourrelly and P. L. Llewellyn, *J. Am. Chem. Soc.*, 2008, **130**, 15967.
83 E. Garrone, B. Bonelli and C. Otero Arean, *Chem. Phys. Lett.*, 2008, **456**, 68.
84 M. S. Westwell, M. S. Searle, J. Klein and D. H. Williams, *J. Phys. Chem.*, 1996, **100**, 16000.
85 A. A. Stolov, W. A. Herrebout and B. J. van der Veken, *J. Am. Chem. Soc.*, 1998, **120**, 7310.
86 D. H. Williams, E. Stephens, D. P. O'Brien and M. Zhou, *Angew. Chem.-Int. Edit.*, 2004, **43**, 6596.
87 G. Sugihara, D. S. Shigematsu, S. Nagadome, S. Lee, Y. Sasaki and H. Igimi, *Langmuir*, 2000, **16**, 1825.
88 X. Solans-Monfort, V. Branchadell, M. Sodupe, C. M. Zicovich-Wilson, E. Gribov, G. Spoto, C. Busco and P. Ugliengo, *J. Phys. Chem. B*, 2004, **108**, 8278.
89 A. Zecchina, S. Bordiga, C. Lamberti, G. Spoto, L. Carnelli and C. O. Arean, *J. Phys. Chem.*, 1994, **98**, 9577.
90 S. Bordiga, C. Lamberti, F. Geobaldo, A. Zecchina, G. T. Palomino and C. O. Arean, *Langmuir*, 1995, **11**, 527.
91 C. Lamberti, S. Bordiga, F. Geobaldo, A. Zecchina and C. O. Arean, *J. Chem. Phys.*, 1995, **103**, 3158.
92 S. Bordiga, E. Garrone, C. Lamberti, A. Zecchina, C. O. Arean, V. B. Kazansky and L. M. Kustov, *J. Chem. Soc.-Faraday Trans.*, 1994, **90**, 3367.
93 K. Sumida, D. Stuck, L. Mino, J.-D. Chai, E. D. Bloch, O. Zavorotynska, L. J. Murray, M. Dinca, S. Chavan, S. Bordiga, M. Head-Gordon and J. R. Long, *J. Am. Chem. Soc.*, 2013, **135**, 1083.
94 C. Otero Arean, M. Rodriguez Delgado, G. Turnes Palomino, M. Tomas Rubio, N. M. Tsyganenko, A. A. Tsyganenko and E. Garrone, *Microporous Mesoporous Mater.*, 2005, **80**, 247.
95 P. Nachtigall, E. Garrone, G. Turnes Palomino, M. Rodriguez Delgado, D. Nachtigallova and C. Otero Arean, *Phys. Chem. Chem. Phys.*, 2006, **8**, 2286.
96 A. Zecchina, S. Bordiga, J. G. Vitillo, G. Ricchiardi, C. Lamberti, G. Spoto, M. Bjorgen and K. P. Lillerud, *J. Am. Chem. Soc.*, 2005, **127**, 6361.
97 G. Turnes Palomino, M. R. Llop Carayol and C. Otero Arean, *J. Mater. Chem.*, 2006, **16**, 2884.
98 G. T. Palomino, B. Bonelli, C. O. Arean, J. B. Parra, M. R. L. Carayol, M. Armandi, C. O. Ania and E. Garrone, *Int. J. Hydrogen Energy*, 2009, **34**, 4371.
99 G. Turnes Palomino, C. Otero Arean and M. R. Llop Carayol, *Appl. Surf. Sci.*, 2010, **256**, 5281.

Electronic Supplementary information

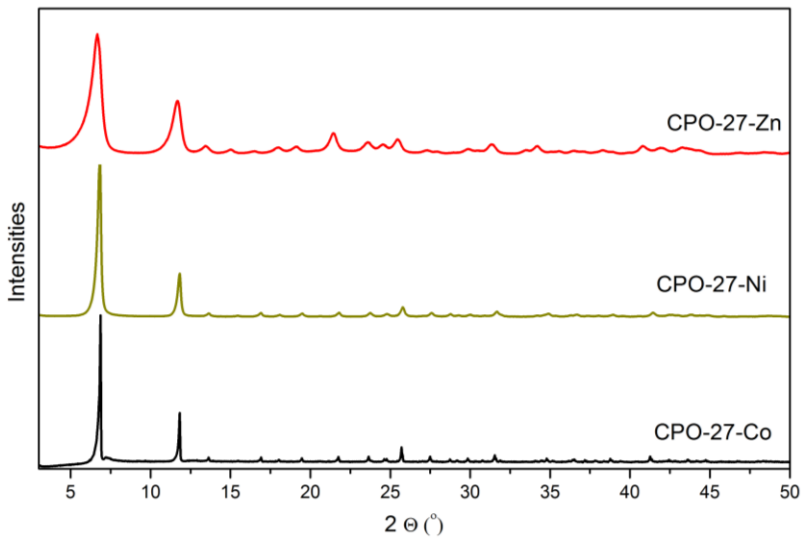

Figure S1. X-ray powder diffraction pattern of in home lab synthesized CPO-27-M (λ = 1.5406 Å).